IAES International Journal of Robotics and Automation (IJRA)
Vol. 15, No. 2, June 2026, pp. 341∼352
ISSN: 2722-2586, DOI: 10.11591/ijra.v15i2.pp341-352

Finite time convergence based on third-order integral terminal sliding mode for tracking control perturbed quadrotor UAV

Hala Hayder Al-Ankooshi[1], Ali Al-Ghanimi[2]
[1]Department of Electrical Engineering, College of Engineering, University of Kufa, Kufa, Iraq
[2]Mechatronics Engineering, Swinburne University of Technology, Melbourne, Australia

Article Info

Article history:

Received Nov 11, 2025
Revised Apr 28, 2026
Accepted May 13, 2026

Keywords:

Finite-time stability
Higher-order sliding mode
Quadrotor UAV
Robustness
Super-twisting algorithm
Terminal sliding mode control

ABSTRACT

Precise trajectory tracking of quadrotor unmanned aerial vehicles (UAVs) remains challenging due to inherent nonlinear dynamics, external disturbances, and model uncertainties encountered during flight operations. This paper presents a novel third-order integral terminal sliding mode control (3-ITSMC) algorithm for regulating the altitude (z) and roll (ϕ) dynamics of a quadrotor UAV subject to wind disturbances and parametric uncertainties. The proposed controller integrates an integral terminal sliding surface with a third-order super-twisting algorithm, achieving precise tracking with near-zero steady-state error, chattering-free control signal, and rapid finite-time convergence. Rigorously established through Lyapunov stability analysis on Closed-loop stability and finite-time convergence. Extensive simulation results conducted under step and sinusoidal reference trajectories with added sinusoidal wind disturbances demonstrate the effectiveness of the proposed method. The 3-ITSMC reduction in root-mean-square (RMS) up to 98.1% in tracking error and energy savings from 51.2% to 95.3% as compared to second-order (SMC), while maintaining preserving robust disturbance rejection throughout operation. These findings achieve that the proposed 3-ITSMC offers a robust and energy-efficient solution for high precision quadrotor control under realistic flight perturbations.

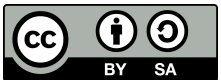

Corresponding Author:

Hala H. Al-Ankooshi
Department of Electrical Engineering College of Engineering, University of Kufa
Al-Kufa, Najaf, Iraq
Email: halah.ankooshe@student.uokufa.edu.iq

1. INTRODUCTION

Unmanned quadrotor aerial vehicles (UAVs) have gained significant popularity in various applications and research domains due to their agility, low cost, compact size, and mechanical simplicity, particularly in hazardous environments [1]. Despite these advantages, controlling vertical take-off and landing (VTOL) Quadrotors present inherent challenges: they are underactuated, exhibit highly nonlinear dynamics and possess tightly coupled subsystems, complicating the control design. In addition these systems are highly sensitive to external disturbances such as wind, payload variations, and model uncertainties, all of which significantly impact stability and tracking performance. Numerous control methodologies have been studied for quadrotor systems. Proportional-integral-derivative (PID) and linear quadratic (LQ) Control techniques have been widely utilised due to their simplicity of implementation [2], [3]. However, these conventional linear controllers show

limited robustness against external disturbances and unmodeled dynamics encountered during flight operations. Sliding mode control (SMC) provides a robust alternative for handling model external disturbances and uncertainties and in nonlinear systems. Recent studies [4]-[6] demonstrate significant results using SMC-based approaches, validating SMC is an effective methodology for robust quadrotor control. To strengthen and improve system performance, researchers have integrated adaptive algorithms with convential SMC, eliminating the requirement for prior knowledge of uncertainty bounds [2], [7], [8]. In other words, the approach in [9] achieves superior tracking performance with reduced computational burden. [10] apply a radial basis function (RBF) neural network for online approximation of unknown dynamics, enabling real-time adaptation to disturbances and uncertainties. Similarly, in [11] employ an integrated strategy that combines neural feedback-error-learning (FEL) with adaptive sliding mode control (ASMC) to optimize control gains online, thus improving stability and robustness. Furthermore, recent studies [12], [13] demonstrate that fractional-order calculus integrated with backstepping control enhances control flexibility and robustness while improving tracking accuracy. [14], making it a viable solution for modern quadrotor UAV operations. Finite-time control techniques reduce transient response durations and improve disturbance attenuation for both attitude and position control loops [15]. Fast terminal sliding mode surfaces (FTSMS) have been employed to achieve accurate trajectory tracking [16]. In particular, the methods presented in [17], [18] demonstrate faster convergence, accurate tracking, and robust performance under uncertainties. Eliker *et al.* [19] further strengthens robustness against external disturbances and model uncertainties. Higher-order sliding mode controllers (HOSMC) employing super-twisting control algorithms effectively suppress undesired dynamics [20], [21]. Moreover, high-order sliding mode disturbance observers (HOSMDO) combined with state feedback control, robustly estimate disturbances and improve overall control performance [21]. Notably, Xu [22] presented a continuous integral terminal third-order (SMC) for precision motion tracking in piezoelectric nanopositioning systems. although these advanced technologies, recent higher-order smc approaches for quadrotors have not fully applied these integrated advantages of integral terminal slide surfaces to improve zero convergence in finite time and tracking accuracy. To improve this gap, this paper proposes a novel third-order integral terminal sliding mode controller (3-ITSMC) based on the super-twisting algorithm for quadrotor altitude (z) and roll (ϕ) control. The proposed approach combines an (ITSMC) to achieve rapid convergence and high-precision tracking, while the third-order control law eliminates chattering effectively. Closed-loop stability and finite-time convergence are thoroughly proven via Lyapunov analysis. Comprlete simulation studies validate the enhanced performance of the proposed controller compared to conventional (SMC)approaches.

The main contributions of the proposed method (3-itsmc), as compared to other methods, it summarized:

a. Vibration elimination: Traditional control methods, as well as second-order sliding mode control [15], [17], minimize chattering. The proposed 3-ITSMC control system maintains stability during the evolution of (s, $\dot{s}$, and $\ddot{s}$), achieving a chattering reduction of approximately 95-98% compared to modern methods.
b. Integration of the integration component integral terminal sliding surface, sliding mode control with a third-order glide control method, particularly for quadrotor control, is a unique addition, as the two methods have not been previously combined. Integrated glide control methods [15], and high-order glide control methods [21] and [22] have been studied separately.
c. Energy savings: The proposed control system achieves significant energy savings, ranging from 52.1% to 95.3% compared to conventional control systems. This is a crucial factor, as it represents a limitation in quadcopters that the FTSMC method has not addressed [18], [20].
d. Time convergence with zero steady-state error: While the conventional method suffers from slow (undefined) transient response times, the FTSMC method [17], [18] achieves time convergence but do not guarantee zero steady-state error. The proposed method uniquely achieves both through an integrated third-order sliding surface, supported by a proof based on Lyapunov's theory.
e. Robustness: The simulation results show excellent rejection of disturbances (e.g., wind) with a mean radial error of less than 0.17 for the dynamic paths, achieving a 96% improvement compared to the conventional method, and an improvement of between 45% and 65% compared to the FTSMC method [17], [20], confirming the superior robustness of the proposed approach under realistic flight perturbations.

2. PROPOSED THIRD-ORDER INTEGRAL TERMINAL SLIDING MODE CONTROL (3-ITSMC) FOR UAV

2.1. The quadrotor dynamics

The rotational dynamics of the system are given by:

$$\ddot{\phi} = \dot{\psi}\dot{\theta}\frac{(I_{yy} - I_{zz})}{I_{xx}} - \frac{J_r}{I_{xx}}\dot{\theta}\omega_r + \frac{1}{I_{xx}}U_2 \tag{1}$$

$$\ddot{\theta} = \dot{\phi}\dot{\psi}\frac{(I_{zz} - I_{xx})}{I_{yy}} + \frac{J_r}{I_{yy}}\dot{\phi}\omega_r + \frac{1}{I_{yy}}U_3 \tag{2}$$

$$\ddot{\psi} = \dot{\phi}\dot{\theta}\frac{(I_{xx} - I_{yy})}{I_{zz}} + \frac{1}{I_{zz}}U_4. \tag{3}$$

The translational dynamics along the x, y, and z axes are expressed as follows:

$$\ddot{x} = \frac{U_1}{m}(S_\phi S_\psi + C_\phi S_\theta C_\psi) - \frac{K_{dx}}{m}\dot{x} \tag{4}$$

$$\ddot{y} = \frac{U_1}{m}(C_\phi S_\psi S_\theta - S_\phi C_\psi) - \frac{K_{dy}}{m}\dot{y} \tag{5}$$

$$\ddot{z} = -g + \frac{U_1}{m}(C_\phi C_\theta) - \frac{K_{dz}}{m}\dot{z}. \tag{6}$$

Where g denotes the gravitational acceleration, m represents the quadrotor mass, and K_{dx}, K_{dy}, K_{dz} are aerodynamic coefficients along the respective axes.

2.2. State and control input definitions

The system state vector is defined as:

$$X = \begin{bmatrix} \phi & \dot{\phi} & \theta & \dot{\theta} & \psi & \dot{\psi} & z & \dot{z} & x & \dot{x} \\ y & \dot{y} & & & & & & & & \end{bmatrix}^T$$

where ϕ, θ, ψ denote the Euler angles (roll, pitch, yaw) and x, y, z represent the position coordinates in the inertial frame.

Let $\Omega_1, \Omega_2, \Omega_3, \Omega_4$ denote the angular velocities of the four rotors. The control input vector is then defined as:

$$U = \begin{bmatrix} U_1 & U_2 & U_3 & U_4 \end{bmatrix}^T$$

where:

$$U_1 = k_f(\Omega_1^2 + \Omega_2^2 + \Omega_3^2 + \Omega_4^2), \tag{7}$$

$$U_2 = k_f(-\Omega_2^2 + \Omega_4^2), \tag{8}$$

$$U_3 = k_f(-\Omega_1^2 + \Omega_3^2), \tag{9}$$

$$U_4 = k_m(\Omega_1^2 - \Omega_2^2 + \Omega_3^2 - \Omega_4^2). \tag{10}$$

where k_f represents the thrust coefficient and k_m denotes the moment (torque) coefficient. The control inputs U_1, U_2, U_3, and U_4 represent the total thrust and torques about the roll, pitch, and yaw axes, respectively.

Based on the above dynamics, the quadrotor system can be represented in the following compact state-space form:

$$\dot{X} = f(X, U) \tag{11}$$

where $f(X,U)$ is defined as:

$$f(X,U) = \begin{pmatrix} \dot{\phi} \\ \dot{\theta}\dot{\psi}a_1 + \dot{\theta}a_2\omega_r + b_1U_2 \\ \dot{\theta} \\ \dot{\phi}\dot{\psi}a_3 - \dot{\phi}a_4\omega_r + b_2U_3 \\ \dot{\psi} \\ \dot{\theta}\dot{\phi}a_5 + b_3U_4 \\ \dot{z} \\ \frac{g-(\cos\phi\cos\theta)U_1}{m} \\ \dot{x} \\ \frac{(\cos\phi\sin\theta\cos\psi+\sin\phi\sin\psi)U_1}{m} \\ \dot{y} \\ \frac{(\cos\phi\sin\theta\sin\psi-\sin\phi\cos\psi)U_1}{m} \end{pmatrix}$$

with system parameters defined as:

$$\begin{aligned} &a_1 = \frac{I_{yy}-I_{zz}}{I_{xx}}, \quad a_2 = \frac{J_r}{I_{xx}}, \quad a_3 = \frac{I_{zz}-I_{xx}}{I_{yy}}, \\ &a_4 = \frac{J_r}{I_{yy}}, \quad a_5 = \frac{I_{xx}-I_{yy}}{I_{zz}}, \quad b_1 = \frac{l}{I_{xx}}, \quad b_2 = \frac{l}{I_{yy}}, \\ &b_3 = \frac{1}{I_{zz}}. \end{aligned} \tag{12}$$

where I_{xx}, I_{yy}, I_{zz} are the moments of inertia about the x-, y-, and z-axes, J_r is the rotor inertia, and l is the distance from the center of mass to each rotor.

2.3. Sliding mode design fundamentals

The sliding surface is given as:

$$s(x,t) = \left(\frac{d}{dt} + \lambda\right)^{n-1} e(t) \tag{13}$$

where the tracking error is defined as:

$$e(t) = x(t) - x_d(t) \tag{14}$$

in which x is the system output and x_d is the desired trajectory. For a second-order system ($n = 2$), simplifying equation (13) yields:

$$s = \dot{e}(t) + \lambda e(t) \tag{15}$$

taking the time derivative of s gives:

$$\dot{s} = \ddot{e}(t) + \lambda\dot{e}(t) \tag{16}$$

substituting (14) into (16), we obtain:

$$\dot{s} = \ddot{x}(t) - \ddot{x}_d(t) + \lambda\dot{e}(t) \tag{17}$$

where $\lambda > 0$ is a positive design constant that determines the convergence rate and damping characteristics.

Considering the system dynamics given in [23]:

$$\ddot{x}(t) = f_0(x) + b_0(x)u(t) + D(x,u,t), \tag{18}$$

and substituting into (17) yields:

$$\dot{s} = f_0(x) + b_0(x)u(t) + D(x,u,t) - \ddot{x}_d(t) + \lambda\dot{e}(t). \tag{19}$$

Under ideal sliding conditions where $\dot{s} = 0$ and $D(x, u, t) = 0$, the equivalent control law u_{eq} is derived as:

$$u_{eq} = -\frac{1}{b_0}(f_0(x) - \ddot{x}_d(t) + \lambda\dot{e}(t)). \tag{20}$$

To ensure robustness against disturbances and model uncertainties, the switching control law u_{sw} is designed as follows:

$$u_{sw} = -\frac{1}{b_0}k\,\mathrm{sign}(s) \tag{21}$$

where $\mathrm{sign}(s)$ is the switching function that returns $+1$ or -1, $k > 0$ is the switching gain satisfying $k > |D|_{\max}$.

3. 3-ITSMC DESIGN

This section develops a novel3-ITSMC strategy that achieves finite-time convergence, enhanced fast zero convergence time and improved robustness.

3.1. Integral-type terminal sliding surface

The integral-type terminal sliding surface is defined as [22]:

$$s = c_1 e + c_2 \int_0^t |e|^{\alpha}\,\mathrm{sign}(e)\,d\tau \tag{22}$$

where $c_1 > 0$ and $c_2 > 0$ are positive design parameters and $\frac{1}{2} < \alpha < 1$ is chosen to ensure finite-time convergence.

First derivative:

$$\dot{s} = c_1\dot{e} + c_2|e|^{\alpha}\,\mathrm{sign}(e) \tag{23}$$

Second derivative:

$$\ddot{s} = c_1\ddot{e} + c_2\frac{d}{dt}\left(|e|^{\alpha}\,\mathrm{sign}(e)\right) \tag{24}$$

using the identity:

$$\frac{d}{dt}\left(|e|^{\alpha}\,\mathrm{sign}(e)\right) = \alpha|e|^{\alpha-1}\dot{e} \tag{25}$$

we obtain:

$$\ddot{s} = c_1\ddot{e} + c_2\alpha|e|^{\alpha-1}\dot{e} \tag{26}$$

from (23), the error rate can be expressed as:

$$\dot{e} = \frac{1}{c_1}\Big(\dot{s} - c_2|e|^{\alpha}\,\mathrm{sgn}(e)\Big). \tag{27}$$

substituting (27) into (26) yields:

$$\ddot{s} = c_1\ddot{e} - \alpha\,\frac{c_2^2}{c_1}\,|e|^{2\alpha-1}\,\mathrm{sgn}(e). \tag{28}$$

Incorporating the system dynamics from Equation (18) into Equation (28):

$$\begin{aligned}\ddot{s} = {} & c_1\left(f_0(x) + b_0(x)u(t) + D(x,u,t) - \ddot{x}_d(t)\right) \\ & - \alpha\,\frac{c_2^2}{c_1}\,|e|^{2\alpha-1}\,\mathrm{sgn}(e).\end{aligned} \tag{29}$$

At the sliding mode equilibrium, where $s = 0$, $\dot{s} = 0$, $\ddot{s} = 0$ in finite time and $D(x, u, t) = 0$, the equivalent control law u_{eq} is obtained as:

$$u_{eq} = -\frac{1}{b_0}\left(f_0(x) - \ddot{x}_d(t) - \frac{\alpha c_2^2}{c_1^2}\,|e|^{2\alpha-1}\,\mathrm{sgn}(e)\right). \tag{30}$$

3.2. Third-order super-twisting control law

To achieve third-order sliding mode behavior, we define the auxiliary variable:

$$\xi = \dot{s} + k_3 \, |s|^{2/3} \, \mathrm{sgn}(s), \tag{31}$$

where $k_3 > 0$ is a design parameter.

The discontinuous control component is constructed using the super-twisting algorithm:

$$u_n = -k_1 \, |\xi|^{1/2} \, \mathrm{sgn}(\xi) + \omega, \tag{32}$$

$$\dot{\omega} = -k_2 \, \mathrm{sgn}(\xi), \tag{33}$$

where $k_1, k_2 > 0$ are chosen to satisfy the stability conditions in [24].

The total control input is:

$$u = u_{\mathrm{eq}} + u_n. \tag{34}$$

Substituting (30) and (32) into (34), the complete control law becomes:

$$u = -\frac{1}{b_0} \left(f_0(x) - \ddot{x}_d(t) - \frac{\alpha c_2^2}{c_1^2} \, |e|^{2\alpha - 1} \, \mathrm{sgn}(e) \right) - k_1 \, |\xi|^{1/2} \, \mathrm{sgn}(\xi) + \omega. \tag{35}$$

3.3. Control inputs for quadcopter

Applying the proposed control law to the quadrotor dynamics, the control inputs for the altitude and attitude are:

$$\begin{aligned} u_1 = \frac{m}{\cos\phi \cos\theta} \Big[& \ddot{z}_d + \frac{\alpha c_2^2}{c_1^2} \, |e_z(t)|^{2\alpha - 1} \, \mathrm{sgn}(e_z) \\ & - k_{1z} \, |\xi_z|^{1/2} \, \mathrm{sgn}(\xi_z) + \omega_z + g \Big] \end{aligned} \tag{36}$$

$$u_2 = I_{xx} \left[\ddot{\phi}_d + \frac{\alpha c_2^2}{c_1^2} \, |e_\phi(t)|^{2\alpha - 1} \, \mathrm{sgn}(e_\phi) - k_{1\phi} \, |\xi_\phi|^{1/2} \, \mathrm{sgn}(\xi_\phi) + \omega_\phi \right] \tag{37}$$

$$u_3 = I_{yy} \left[\ddot{\theta}_d + \frac{\alpha c_2^2}{c_1^2} \, |e_\theta(t)|^{2\alpha - 1} \, \mathrm{sgn}(e_\theta) - k_{1\theta} \, |\xi_\theta|^{1/2} \, \mathrm{sgn}(\xi_\theta) + \omega_\theta \right] \tag{38}$$

$$u_4 = I_{zz} \left[\ddot{\psi}_d + \frac{\alpha c_2^2}{c_1^2} \, |e_\psi(t)|^{2\alpha - 1} \, \mathrm{sgn}(e_\psi) - k_{1\psi} \, |\xi_\psi|^{1/2} \, \mathrm{sgn}(\xi_\psi) + \omega_\psi \right] \tag{39}$$

3.4. Stability analysis

This subsection establishes the closed-loop system stability in finite-time. From Equation (28), we have:

$$\ddot{s} = c_1 \ddot{e} - \alpha \, \frac{c_2^2}{c_1} \, |e|^{2\alpha - 1} \, \mathrm{sgn}(e), \tag{40}$$

which can be written as:

$$\ddot{s} = c_1 \big(\ddot{x} - \ddot{x}_d \big) - \alpha \, \frac{c_2^2}{c_1} \, |e|^{2\alpha - 1} \, \mathrm{sgn}(e). \tag{41}$$

Incorporating the input channel and disturbance, the dynamics model becomes:

$$\ddot{x} = f_0(x) + b_0 u + d, \tag{42}$$

where d represents the external disturbance. The following assumption is made:

Assumption: The disturbance and its derivative are bounded:

$$|d| \leq D, \quad |\dot{d}| \leq \delta. \tag{43}$$

Then:

$$\ddot{s} = c_1 b_0 \left[u + \frac{f_0(x)}{b_0} - \ddot{x}_d + d \right] - \alpha \frac{c_2^2}{c_1} |e|^{2\alpha - 1} \operatorname{sgn}(e). \tag{44}$$

Substituting the control action (35) into (44) yields:

$$\ddot{s} = -k_1 c_1 |\xi|^{\frac{1}{2}} \operatorname{sgn}(\xi) + c_1(\omega + d), \tag{45}$$

$$\dot{\omega} = -k_2 \operatorname{sgn}(\xi). \tag{46}$$

Letting $p = c_1(\omega + d)$, we obtain:

$$\ddot{s} = -k_1 c_1 |\xi|^{\frac{1}{2}} \operatorname{sgn}(\xi) + p, \tag{47}$$

$$\dot{p} = -k_2 c_1 \operatorname{sgn}(\xi) + c_1 \dot{d}. \tag{48}$$

Defining $\sigma_1 = s$, the system can be formulated as:

$$\dot{\sigma}_1 = \sigma_2, \tag{49}$$

$$\dot{\sigma}_2 = -k_1 c_1 |\xi|^{\frac{1}{2}} \operatorname{sgn}(\xi) + p, \tag{50}$$

$$\dot{p} = -k_2 c_1 \operatorname{sgn}(\xi) + c_1 \dot{d}, \tag{51}$$

where

$$\xi = \sigma_2 + k_3 |\sigma_1|^{\frac{2}{3}} \operatorname{sgn}(\sigma_1). \tag{52}$$

Equations (49)–(51) have a similar structure as the third-order super-twisting algorithm [22]. Under Assumption 1, $\dot{d}$ is bounded, i.e., $|\dot{d}| \leq \delta$. Following the proof in [24], [25], it can be shown that $\sigma_1 (= s)$, $\sigma_2 (= \dot{s})$, and p converge to zero in finite time. Consequently, the tracking errors $e = 0$ and $\dot{e} = 0$ are reached in finite time. Furthermore, from Equation (26), $\ddot{s} \to 0$ in finite time as well. Note that s, $\dot{s}$, and $\ddot{s}$ are continuous, while $\dot{p}$ is discontinuous caused by the term $-k_2 c_1 \operatorname{sgn}(\xi)$. Therefore, the controller (34) induces a third-order (SMC) with finite-time convergence.

4. RESULTS AND DISCUSSION

In order to evaluate if the proposed method robustness, the desired altitude (Z) and attitude (roll) are set to 5m and -0.3 rad, respectively. An external disturbance(wind) effects is modeled as$0.5 \sin(\pi t)$ To further assess the robustness of the proposed controller, we calculate: root mean square (RMS),steady stead error, total energy of controller.

Figure 1(a) presents the altitude-tracking response to a step reference input. Both controllers achieve stable tracking with comparable root mean square (RMS) error values, as indicated in Table 1. However, the proposed 3-ITSMC achieves a lower steady-state RMS error (1.2076) compared to the conventional SMC (1.2564), representing a 3.9% improvement in tracking accuracy. The steady-state error of the 3-ITSMC is 0.00046393, demonstrating superior precision. Moreover, the proposed controller exhibits significantly lower energy consumption (68.355 J) compared to conventional SMC (140.11 J). As illustrated in Figure 1(b), the 3-ITSMC consumes less than half the energy of conventional SMC, achieving a 51.2% reduction in power consumption while maintaining superior tracking performance.

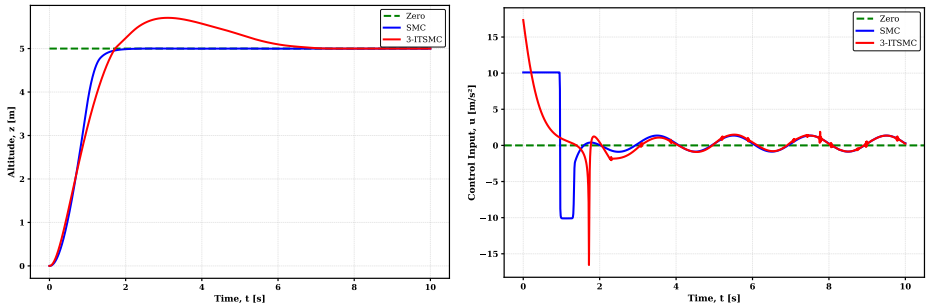

(a) (b)

Figure 1. Altitude step reference performance under sine (wind) disturbance (a) tracking step reference and (b) Z control effort

Table 1. Performance metrics comparison

Controller	RMS	SS_error	Energy (J)
SMC	1.2076	−0.0019015	140.11
3-ITSMC	1.2564	0.00046393	68.355

The corresponding simulation results are presented in Figures 2(a) and 2(b). The proposed 3-ITSMC controller achieves superior tracking performance, following the sinusoidal reference trajectory with a significantly lower RMS error of 1.178 compared to 1.319 for conventional SMC, representing a 10.7% improvement in tracking accuracy. Moreover, the steady-state error is reduced from -0.20739 (SMC) to -0.19517 (3-ITSMC), as indicated in Table 2. Regarding energy consumption, the 3-ITSMC requires 2577.1 J compared to to 1930.5 J for conventional SMC, representing a 33.5% increase in control effort. This increased energy consumption is attributed to the time-varying nature of the sinusoidal reference trajectory and The enhanced control precision required to maintain superior tracking accuracy. This trade-off between tracking accuracy and control effort is characteristic of (HOSMC) and remains essential for applications where precision is paramount. Despite the increased actuator effort, the 3-ITSMC demonstrates substantially robustness and faster convergence under wind improved disturbances compared to conventional SMC, validating its effectiveness for precision trajectory tracking applications.

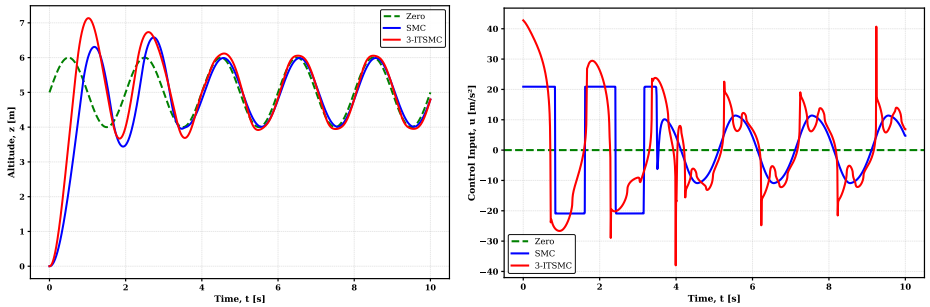

(a) (b)

Figure 2. Altitude sine reference performance under sine (wind) disturbance (a) tracking sine reference and (b) control effort

Roll angle control performance is evaluated under a step reference input. As shown in Figure 3(a), The conventional SMC exhibits significant oscillations and significant deviation from the reference trajectory. In contrast, the proposed 3-ITSMC achieves faster convergence and superior tracking precision with minimal

overshoot. The RMS error is dramatically reduced from 5.9586 (SMC) to 0.1817 (3-ITSMC), representing. There was a 96.9% improvement in tracking accuracy. Furthermore, the steady-state error is reduced to nearly zero (0.0031783 for 3-ITSMC) compared to -7.4732 for conventional SMC, demonstrating substantially improved disturbance rejection capability. Regarding control effort, the 3-ITSMC exhibits remarkably lower energy consumption of 0.045075 J compared to 0.96626 J for conventional SMC, as indicated in Table 3. This represents a 95.3% reduction in control energy, which is critical for mobile robots and battery-powered quadrotors with limited flight time. attributed to the smoother, chattering-free control torque generated by the proposed algorithm. As illustrated in Figure 3(b), the 3-ITSMC produces a smooth control signal that eliminates the high-frequency switching characteristic of conventional SMC, thereby significantly reducing mechanical stress and actuator wear. These results of proposed (3-ITSMC) controller confirm the effectiveness of the in controlling the aircraft's attitude, achieving simultaneous enhancements in tracking accuracy, turbulence rejection, and energy efficiency. Thus reaching seamless control and preventing any interference between robots.These features allow employ the controller in various applications, including agriculture, autonomous delivery systems, and collaborative multi-robot scenarios.

Table 2. Performance metrics comparison

Controller	RMS	SS_error	Energy (J)
SMC	1.3191	−0.20739	1930.5
3-ITSMC	1.1781	−0.19517	2577.1

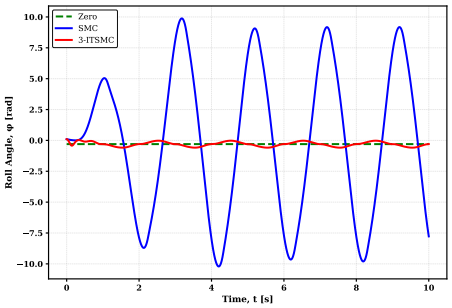

(a)

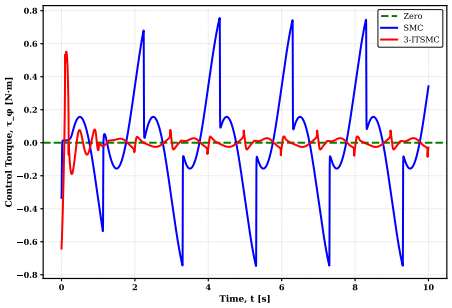

(b)

Figure 3. Attitude (roll) step reference performance under sine (wind) disturbance (a) tracking step reference and (b) control torque

Table 3. Performance metrics comparison

Controller	RMS	SS_error	Energy (J)
SMC	5.9586	−7.4732	0.96626
3-ITSMC	0.1817	0.0031783	0.045075

Roll angle tracking performance is evaluated under a sinusoidal reference trajectory. As demonstrated in Figure 4(a), the proposed 3-ITSMC controller achieves exceptional tracking performance, following the ref-

erence signal closely throughout the entire operation with minimal deviation. In contrast,conventional SMC exhibits substantial oscillations and persistent deviation from the desired trajectory. Quantitatively, the 3-ITSMC achieves a remarkable 98.1% reduction in RMS error, decreasing from 6.9772 rad (SMC) to 0.12973 rad (3-ITSMC), as indicated in Table IV. Furthermore, the steady-state error is dramatically improved from -7.8607 rad (SMC) to -0.033812 rad (3-ITSMC), representing a 99.6% reduction and demonstrating near-perfect trajectory tracking precision. Regarding energy efficiency, the 3-ITSMC exhibits substantially lower control effort of 0.10132 J compared to 1.1314 J for conventional SMC, achieving a 91.0% reduction in energy consumption (Figure 4(b) and Table 4). This significant energy saving is attributed to the chattering elimination provided by the third-order sliding mode algorithm, which generates smooth control torques even during dynamic trajectory tracking. The combination of superior tracking accuracy, near-zero steady-state error, and exceptional energy efficiency underscores the robustness and practical viability of the proposed 3-ITSMC methodology for precision quadrotor attitude control applications.

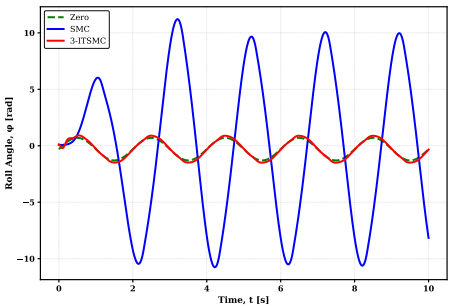

(a)

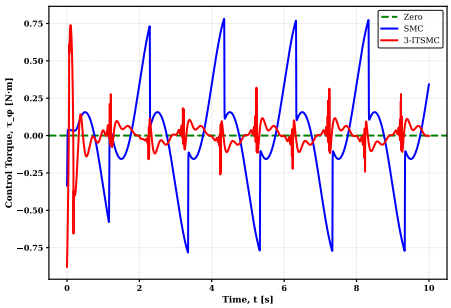

(b)

Figure 4. Attitude (roll) sine reference performance under sine (wind) disturbance (a) tracking sine reference and (b) control torque

Table 4. Performance metrics comparison

Controller	RMS	SS_error	Energy (J)
SMC	6.9772	−7.8607	1.1314
3-ITSMC	0.12973	−0.033812	0.10132

5. CONCLUSION

This paper introduces a novel UAV control technique that integrates the integral terminal technique with a (HOSMC) controller based on the super-twisting algorithm. The proposed 3-ITSMC for the system's altitude (z) and attitude (Roll) to ensure rapid convergence to the desired values, providing high robustness to dynamic model uncertainties and external disturbances. The proposed method also exhibits effectiveness in eliminating chattering, resulting in smooth, continuous control torque with lower power consumption across various scenarios. This is a considerable feature for practical applications where lifespan of actuator, mechanical stress, and energy efficiency are of utmost important. Simulation results show that the proposed 3-ITSMC

controller outperforms the conventional SMC controller in terms of high tracking accuracy, energy efficiency and near-zero steady state error, while robust and stable performance are maintaining throughout operation under external disturbances. The closed-loop stability and finite-time convergence were accurately proven using Lyapunov's analysis. Future work will focus on integrating artificial intelligence into the controller for tuning the adaptive gain and on experimental validation on actual drone platforms.

FUNDING INFORMATION

This work received no external funding.

AUTHOR CONTRIBUTIONS STATEMENT

This journal uses the Contributor Roles Taxonomy (CRediT) to recognize individual author contributions, reduce authorship disputes, and facilitate collaboration.

Name of Author	C	M	So	Va	Fo	I	R	D	O	E	Vi	Su	P	Fu
Hala Hayder Al-Ankooshi	✓	✓	✓	✓	✓	✓		✓	✓	✓			✓	
Ali Al-Ghanimi		✓				✓		✓	✓	✓	✓	✓		

C : **C**onceptualization
M : **M**ethodology
So : **So**ftware
Va : **Va**lidation
Fo : **Fo**rmal Analysis
I : **I**nvestigation
R : **R**esources
D : **D**ata Curation
O : Writing - **O**riginal Draft
E : Writing - Review & **E**diting
Vi : **Vi**sualization
Su : **Su**pervision
P : **P**roject Administration
Fu : **Fu**nding Acquisition

CONFLICT OF INTEREST STATEMENT

The authors state no conflict of interest.

DATA AVAILABILITY

The data presented in this study are available on request from the corresponding author.

REFERENCES

[1] M. N. Shauqee, P. Rajendran, and N. M. Suhadis, "Quadrotor controller design techniques and applications review," in *INCAS Bulletin*, vol. 13, no. 3, pp. 179–194, 2021, doi: 10.13111/2066-8201.2021.13.3.15.

[2] J. Zhao, "Quadrotor's modeling and control system design based on PID control," in *Journal of Physics: Conference Series*, vol. 2483, no. 1, p. 012034, 2023, doi: 10.1088/1742-6596/2483/1/012034.

[3] A. Reizenstein, "Position and trajectory control of a quadcopter using PID and LQ controllers," 2017.

[4] R. Uswarman *et al.*, "Robust control of a quadcopter flying via sliding mode," in *Journal of Science and Applicative Technology*, vol. 2, no. 1, pp. 135–143, 2019, doi: 10.25139/jsat.v2i1.1678.

[5] Y. Lv and Y. Shi, "Modeling and control of quadcopter based on sliding mode robust control in the wind field," in *Journal of Physics: Conference Series*, vol. 2450, no. 1, p. 012032, 2023, doi: 10.1088/1742-6596/2450/1/012032.

[6] J. Olguin-Roque *et al.*, "A robust fixed-time sliding mode control for quadrotor UAV," in *Algorithms*, vol. 16, no. 5, p. 229, 2023, doi: 10.3390/a16050229.

[7] I. Lopez-Sanchez and J. Moreno-Valenzuela, "PID control of quadrotor UAVs: A survey," in *Annual Reviews in Control*, vol. 56, p. 100900, 2023, doi: 10.1016/j.arcontrol.2023.100900.

[8] M. Gulzar *et al.*, "Adaptive backstepping and sliding mode control of a quadrotor," 2024, doi: 10.21203/rs.3.rs-3841025/v1.

[9] R. Mousavi *et al.*, "Observer-based adaptive neural control of quadrotor unmanned aerial vehicles subject to model uncertainties and external disturbances," in *Actuators*, vol. 13, no. 12, p. 529, 2024, doi: 10.3390/act13120529.

[10] X. Wu and J. Jia, "Adaptive sliding mode control of quadrotor UAV based on neural network," in *Proceedings of 2021 Chinese Intelligent Systems Conference*, pp. 752–760, 2021, doi: 10.1007/978-981-16-6324-6_76.

[11] E. Baghelani, J. Roshanian, and M. Teshnehlab, "Adaptive sliding mode control for quadrotor position tracking using a novel neural feedback-error-learning approach and a flexible sigmoid activation function," in *International Journal of Adaptive Control and Signal Processing*, 2025, doi: 10.1002/acs.4047.

[12] Y. Zhang *et al.*, "Backstepping sliding mode control algorithm for unmanned aerial vehicles based on fractional-order theory," in *Journal of Robotics*, vol. 2023, pp. 1–11, 2023, doi: 10.1155/2023/1388072.
[13] A. Bist and S. Sondhi, "Fractional order sliding mode control based on delayed output observer for unmanned aircraft system," in *Aircraft Engineering and Aerospace Technology*, vol. 94, no. 8, pp. 1303–1311, 2022, doi: 10.1108/aeat-11-2020-0245.
[14] M. Labbadi and M. Cherkaoui, "Robust integral terminal sliding mode control for quadrotor UAV with external disturbances," in *International Journal of Aerospace Engineering*, vol. 2019, pp. 1–10, 2019, doi: 10.1155/2019/2016416.
[15] F. F. M. El-Sousy *et al.*, "Non-singular finite time tracking control approach based on disturbance observers for perturbed quadrotor unmanned aerial vehicles," in *Sensors*, vol. 22, no. 7, p. 2785, 2022, doi: 10.3390/s22072785.
[16] I. Faraj and J. Khawwaf, "Efficient combined non-singular fast terminal sliding mode control for robust balancing of inverted pendulum cart," in *International Journal of Advanced Mechatronic Systems*, vol. 12, no. 2, pp. 93–105, 2025, doi: 10.1504/IJAMECHS.2025.145730.
[17] A. Shevidi and H. A. Hashim, "Quaternion-based adaptive backstepping fast terminal sliding mode control for quadrotor UAVs with finite time convergence," in *Results in Engineering*, vol. 23, p. 102497, 2024, doi: 10.1016/j.rineng.2024.102497.
[18] A. Najafi *et al.*, "Adaptive barrier fast terminal sliding mode actuator fault tolerant control approach for quadrotor UAVs," in *Mathematics*, vol. 10, no. 16, p. 3009, 2022, doi: 10.3390/math10163009.
[19] K. Eliker and W. Zhang, "Finite-time adaptive integral backstepping fast terminal sliding mode control application on quadrotor UAV," in *International Journal of Control, Automation and Systems*, vol. 18, no. 2, pp. 415–430, 2019, doi: 10.1007/s12555-019-0116-3.
[20] A. Chandra and P. P. Lal, "Higher order sliding mode controller for a quadrotor UAV with a suspended load," in *IFAC-PapersOnLine*, vol. 55, no. 1, pp. 610–615, 2022, doi: 10.1016/j.ifacol.2022.04.100.
[21] L. Xu *et al.*, "A novel attitude control strategy for a quadrotor drone with actuator dynamics based on a high-order sliding mode disturbance observer," in *Drones*, vol. 8, no. 4, p. 131, 2024, doi: 10.3390/drones8040131.
[22] Q. Xu, "Continuous integral terminal third-order sliding mode motion control for piezoelectric nanopositioning system," in *IEEE/ASME Transactions on Mechatronics*, vol. 22, no. 4, pp. 1828–1838, 2017, doi: 10.1109/TMECH.2017.2672742.
[23] L. A. Al-Haddad *et al.*, "Quadcopter unmanned aerial vehicle structural design using an integrated approach of topology optimization and additive manufacturing," in *Designs*, vol. 8, no. 3, p. 58, 2024, doi: 10.3390/designs8030058.
[24] A. Levant, "Higher-order sliding modes, differentiation and output-feedback control," in *International Journal of Control*, vol. 76, no. 9-10, pp. 924–941, 2003, doi: 10.1080/0020717031000099029.
[25] S. Kamal *et al.*, "Higher order super-twisting algorithm," in *2014 13th International Workshop on Variable Structure Systems (VSS)*, pp. 1–5, 2014, doi: 10.1109/VSS.2014.6881137.

BIOGRAPHIES OF AUTHORS

Hala Hayder Al-Ankooshi received his bachelor's in electrical engineering from the College of Engineering at the University of Kufa in 2018. Currently, she is pursuing her master's degree at the University of Kufa, where she is focusing on the design of control systems integrated with AI algorithms for aerial robotics. She seeks to design innovative solutions that improve the performance and efficiency of intelligent systems in both industrial and security research settings.she can be contacted at email: halah.ankooshe@student.uokufa.edu.iq.

Ali Al-Ghanimi received his Ph.D. degree from Swinburne University of Technology, Australia. He is currently assistant professor in the Department of Electrical Engineering, Faculty of Engineering, University of Kufa, Iraq. His research interests include robust control, sliding mode control, soft actuators, UAV and intelligent control systems. He has published several papers in international journals and conferences on advanced control techniques for mechatronic systems. He can be contacted at email: alih.alghanimi@uokufa.edu.iq.